



Suction and Lorentz force effects on MHD free convective transport of micropolar fluid passing a Unsteady analysis

Md. Abul Kalam Azad ^a, Md. Hasanuzzaman ^{a,*}, Md. Mosharof Hossain ^b, Akio Miyara ^{c,d}

^a Department of Mathematics, Khulna University of Engineering & Technology, Khulna 9203, Bangladesh

^b Department of Mathematics, Bangladesh University of Engineering and Technology, Dhaka 1000, Bangladesh

^c Department of Mechanical Engineering, Saga University, Saga-shi 840-8502, Japan

^d International Institute for Carbon-Neutral Energy Research, Kyushu University, Fukuoka-shi 819-0395, Japan

ARTICLE INFO

Keywords:

MHD
Micropolar fluid
Force convection
Heat transfer
Mass transfer
Porous medium

ABSTRACT

A comprehensive study of the nature of micropolar fluid on an unsteady MHD-free convective transference through a perforated sheet is discussed considering the suction and Lorentz's force effects. The corresponding similarity equations of temperature, momentum, concentration, and angular momentum equations have been modified into the non-dimensional similarity equations of the temperature, momentum, concentration, and angular momentum equations by utilizing the similarity technique. The modified equations have been resolved by exerting the shooting technique with the help of the finite difference method (FDM) through MATLAB. The fluid flow is inversely proportional to the changes in micro rotational effect (Δ). The concentration boundary layer gets thinner as the Schmidt number (Sc) advances and hence the concentration of the fluid decreases. Micropolar fluid helps reduce drag forces and also acts as a coolant. The heat transmission rate advances by around 391%, and 110% due to growing amounts of Pr from 0.71 to 7.0, and v_0 from 0.6 to 3.0, respectively. The surface couple stress decays by about 33%, 45%, and 36% due to increasing values of M from 0.6 to 3.6, Δ from 3.0 to 6.0, and λ from 0.1 to 1.2, respectively.

1. Introduction

The fluids including the microstructure are micropolar fluids. In industries and engineering processes, many non-Newtonian liquids are ordinary to move across a vertical plate which is not possible to explain by a linear relationship between rate of deformation and stress. Fossil fuels, molten polymers, pulps, fluids, and animal blood which contain assured preservatives, etc. are examples of such fluids that sometimes are found in industrial production. Among the several non-Newtonian fluids model, the basic theory of molecular fluids has been studied for the last few years as this type of fluids illustrates, body fluids, a lot of industrial important fields related to paints, colloidal fluids, polymers, animal blood, suspension fluids, liquid crystal, etc. been developed by Eringen [1]. Physically, with the big dumbbell-shaped molecules can form a cylindrical material in micropolar fluids, suspension of small, rigid. The idea of moving surfaces like filaments polymer sheets always drawn as of die has been earlier introduced by Sakiadis [2]. He has explained how the boundary layer behaves on a range of solid, level surfaces. There are many researchers have explained the boundary layer

flow as a significant kind of flow in various technical systems, like the production of glass fiber, paper dying and textiles, continuous casting, hot rolling, etc. When the micro-inertia is variable, then a possible similarity solution of micropolar boundary layer movement over a sheet has been discussed by Ahmadi [3]. Jena and Mathur [4] have studied the flow of the laminar natural convection of thermo-micro polar fluids past in a non-isothermal vertical sheet in detail. Ojjela and Naresh Kumar [5] explored the unstable MHD transport of micropolar liquid past in a perforated medium between parallel sheets. Ashraf and Wehgal [6] examined the role of a uniform magnetic field upon steady incompressible heat transmission movement of electrically conducting micropolar liquid between two stationary infinite parallel permeable plates. The analytic solution for time-dependent magnetohydrodynamics (MHD) boundary layer movement of micropolar liquids passing a perforated medium was discussed by Nadeem et al. [7]. Rahman and Sattar [8] explained the influence of heat absorption/ production on MHD convective micropolar fluid flow through a continuously moving vertical permeable plate. The influences of radiative on the stable MHD combined convective stagnation point movement towards a vertical plate involved with incompressible micropolar liquid have been

* Corresponding author.

E-mail address: hasanuzzaman@math.kuet.ac.bd (Md. Hasanuzzaman).

<https://doi.org/10.1016/j.aej.2024.04.067>

Received 8 November 2023; Received in revised form 28 February 2024; Accepted 27 April 2024

Available online 18 May 2024

1110-0168/© 2024 The Author(s). Published by Elsevier BV on behalf of Faculty of Engineering, Alexandria University This is an open access article under the CC BY-NC-ND license (<http://creativecommons.org/licenses/by-nc-nd/4.0/>).

Nomenclature			
MHD	magnetohydrodynamic	χ	vortex viscosity parameter
j	square of characteristic length of microstructure	ρ	density of base fluid, kg m^{-3}
u	velocity component across x-axis, ms^{-1}	B_0	uniform transverse magnetic field strength, Am^{-1}
C	Particle concentration kgm^{-3}	v	velocity component across y-axis, ms^{-1}
C_W	surface concentration kgm^{-3}	T	fluid temperature, k^{-1}
C_∞	Free stream concentration, kgm^{-3}	T_W	surface temperature, k^{-1}
τ	vortex viscosity	T_∞	free stream temperature, k^{-1}
β	coefficient of volumetric expansion	g	gravitational acceleration, ms^{-2}
D_m	coefficient of mass diffusivity, L^2T^{-1}	ν	Kinematic viscosity m^2s^{-1}
P_r	Prandtl number	k_T	thermal diffusion ratio
G_m	modified local Grashof Number	N	Angular momentum, $\text{KgM}^2\text{T}^{-1}$
Sc	Schmidt number	G_r	local Grashof number
Λ	spin gradient viscosity, $\text{ML}^{-1}\text{T}^{-1}$	λ_1	arbitrary constant
λ	vortex viscosity, $\text{ML}^{-1}\text{T}^{-1}$	Δ	micro rotational parameter
h	dimensionless micro-rotation	U	dimensionless velocity
C_f	local skin friction	θ	dimensionless temperature
N_u	local Nusselt number	ϕ	dimensionless concentration
β^*	coefficient of volumetric expansion with concentration	S_h	local Sherwood number
U_0	uniform velocity at free stream	μ	Dynamic viscosity, $\text{ML}^{-1}\text{T}^{-1}$
		ω	Activation energy parameter
		s	constant

discussed by Olanrewaju et al. [9].

Soret and Dufour are two related phenomena in heat transmission as well as fluid dynamics, particularly in the context of mass and heat transport in fluid systems. They are often associated with the study of convection, which is the transmission of heat and mass within a fluid due to both bulk motion (advection) and diffusion. The Soret effect, also known as thermal diffusion, is a phenomenon where there is a preferential diffusion of one component of a mixture in response to a temperature gradient. In simpler terms, it means that when a temperature difference is applied to a mixture of gases or liquids, the individual components of the mixture will move at different rates. The Dufour effect, also known as species diffusion, is a phenomenon where there exists a coupling between heat transmission and mass transmission in a fluid flow. In other words, when a fluid experiences a temperature gradient, it can induce a mass transfer (diffusion) of the fluid components. Recently, Hasanuzzaman et al. [10] explored the unstable MHD free convection transport on a vertical perforated sheet with Dufour and thermal diffusion influences. Then, Hasanuzzaman et al. [10,11] enlarged the investigation of Hasanuzzaman et al. [10] by considering the chemical reactions, thermal radiation, and heat production, respectively. The influence of Soret and viscous dissipation on stable MHD-free convective transportation over a vertical perforated plate in a perforated medium was analyzed by Reddy and Reddy [12]. The important roles of the chemical reaction and Soret and Dufour on MHD convective transport of an incompressible micropolar fluid over the perforated medium between two parallel sheets have been explained by Ojjela and Naresh [13]. Sheri and Shamshuddin [15] viewed the roles of viscous dissipation on micropolar liquid's MHD flow via a stretched sheet with the chemical reaction effect. Heat transportation and micropolar fluid movement in a perforated channel were considered by Mirgolbabaee et al. [14]. A numerical solution for mass and heat transmission within the incompressible micropolar viscous fluid movement by a resisted perforated medium within the channel with flat walls has been analyzed by Ahmad et al. [15]. Ghoneim et al. [16] examined the influence of a squeezing motion on the magnetohydrodynamic (MHD) of Darcy–Forchheimer nanofluids past in host fluid water flow. The intelligent computational strength of neural networks based on the Levenberg–Marquardt backpropagation (LMBP-NNs) neural networks technique for the simulation of Maxwell nanofluid flow past a linear stretchable surface model has been explored by Khan et al. [17]. Hosseini et al. [18] explored the reliability of the mentioned method by

comparing it with fully solved CFD simulations. The effects of the uniform magnetic influence and thermal radiation on the thermo-gravitational transmission of micropolar nanofluid within a porous chamber have been investigated by Izadi et al. [19]. Krishna et al. [20] studied the influences of the mass and heat transfer on the natural convective flow of micropolar fluid over a vertical perforated sheet. They considered an inclined magnetic field in their simulation. The physical flow of blood in a microcirculatory system by taking account of the particle size effect has been motivated by Krishna et al. [21]. Pattnaik et al. [22] presented the natural convection of an electrically conducting micropolar fluid past a perforated stretching surface. The effects of the Joule, viscous, and Darcy dissipations on the energy transfer flow of a magneto-micropolar nanofluid past a stretchable surface were explained by Mathur et al. [23]. Haque et al. [24] explained the micropolar fluid behavior on steady MHD natural convection and mass transfer through a perforated medium with fixed mass and heat fluxes. We enlarged Hasanuzzaman et al. [10] by considering the angular momentum equation (micropolar fluid).

The key objective of this study is to investigate the roles of the Dufour and Soret on a micropolar fluid movement in a permeable sheet which is the theoretical study. Because there is insufficient experimental data on micropolar fluids. Using similarity conversions, the governing partial differential equations (PDEs) are reformed into non-dimensional ordinary differential equations (ODEs). We resolved the ODEs by the Finite Difference Method (FDM) and then applied MATLAB coding with the shooting method. The angular momentum, velocity, concentration, and temperature are explained graphically for various quantities of the non-dimensional parameters/numbers. The physical parameters such as the local skin friction, and heat and mass transmission rates are incorporated in the tabular forms. Good agreement is found between the comparison outcomes.

The following queries to develop the novelty of the research:

- How does Lorentz's force affect the velocity distribution?
- How does the suction affect the concentration, microrotation, velocity, and temperature profiles?
- How do the micro rotational parameter, and vortex viscosity influence the microrotation, concentration, velocity, and temperature profiles?
- What is the superiority of finite difference method compared with other published paper?

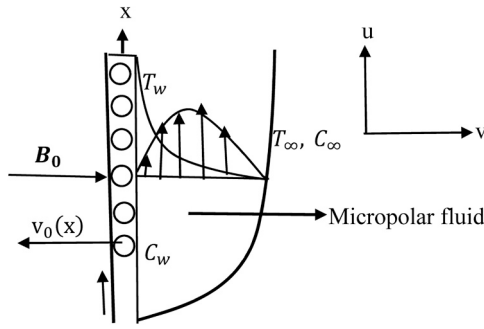


Fig. 1. Physical model and coordinate systems.

2. Mathematics model and governing equations

Let us considered that there is an incompressible, viscous, electrically conducting Micropolar fluid flowing in an unsteady 2D hydromagnetic convective boundary layer over a vertical permeable plate immersed in a permeable medium. The plate is placed across the x -axis. The vertical porous plate and the free-stream velocity are thought to be parallel. It is believed that the vertical porous sheet is normal along the y -axis. A uniform magnetic field of strength $\mathbf{B} = (0, B_0)$ is applied transversely along the flow. Here, C_w and T_w respectively represent the fluid concentration and temperature at the wall. For $t > 0$, the perforated surface inaugurates passing emotively with velocity U in its proper surface. We believe there is an infinite permeable plate. Consequently, $\frac{\partial u}{\partial x} \rightarrow 0$ as $x \rightarrow \infty$. The fluid velocity vector is hence $\vec{q} = u(y, t) \vec{i} + v(y, t) \vec{j}$. The fluid density remains uniform throughout the whole simulation, based on the Boussinesq approximation. (Fig. 1)

According to the Boussinesq approximation and from the above considerations, the two-dimensional governing equations are (Hasanuzzaman et al. [10]):

The continuity equation

$$\frac{\partial v}{\partial y} = 0 \quad (1)$$

The momentum equation

$$\frac{\partial u}{\partial t} + v \frac{\partial u}{\partial y} = \left(\nu + \frac{\chi}{\rho} \right) \frac{\partial^2 u}{\partial y^2} + \frac{\chi}{\rho} \frac{\partial N}{\partial y} + g\beta(T - T_\infty) + g\beta^*(C - C_\infty) - \frac{\sigma B_0}{\nu} u \quad (2)$$

The angular momentum equation:

$$\frac{\partial N}{\partial t} - v_0 \frac{\partial N}{\partial y} = \frac{\gamma}{\rho j} \frac{\partial^2 N}{\partial y^2} - \frac{\chi}{\rho j} \left(2N + \frac{\partial u}{\partial y} \right) \quad (3)$$

The energy equation:

$$\frac{\partial T}{\partial t} - v_0 \frac{\partial T}{\partial y} = \frac{k}{\rho C_p} \frac{\partial^2 T}{\partial y^2} + \frac{D_m k_T}{C_s C_p} \frac{\partial^2 C}{\partial y^2} \quad (4)$$

The concentration equation:

$$\frac{\partial C}{\partial t} - v_0 \frac{\partial C}{\partial y} = D_m \frac{\partial^2 C}{\partial y^2} + \frac{D_m k_T}{T_m} \frac{\partial^2 T}{\partial y^2} \quad (5)$$

The related boundary conditions are-

$$u = U_0(t), v = -v_0, N = -s \frac{\partial u}{\partial y}, T = T_w, C = C_w \text{ at } y = 0 \quad (6)$$

$$u = 0, T \rightarrow T_\infty, N = 0, C \rightarrow C_\infty \text{ at } y \rightarrow \infty \quad (7)$$

where C = fluid concentration, u = velocity component in the x -axis, N = angular momentum, v = velocity component in the y -axis, T = fluid temperature, j = square of the characteristic length of micro-structure, β^* = volumetric coefficient of expansion with concentration, g

= acceleration due to gravity, T_w = surface temperature, t = time, ρ = fluid density, k = thermal conductivity of the medium, T_∞ = free stream temperature, μ = fluid viscosity, C_w = surface concentration, C_∞ = free stream concentration, C_p = specific heat at constant pressure, β = coefficient of volumetric expansion, D_m = coefficient of mass diffusivity, k_T = ratio of thermal diffusion, χ = vortex viscosity parameter, and Other symbols indicate what they usually mean.

Upon introducing the following similarity variables

$$\eta = \frac{y}{\sigma}, f(\eta) = \frac{u}{U}, \tau = \frac{tU_0^2}{\nu}, h(\eta) = \frac{N\nu}{U_0^2}, \theta(\eta) = \frac{T - T_\infty}{T_w - T_\infty}, \phi(\eta) = \frac{C - C_\infty}{C_w - C_\infty} \quad (8)$$

We utilized the time-dependent length scale (σ)

$$\sigma = \sigma(t) \quad (9)$$

where σ is the similarity parameter.

The solution of continuity Eq. (1) is imposed by σ as:

$$v = -v_0 \frac{\nu}{\sigma} \quad (10)$$

Here v_0 represents the dimensionless normal velocity of the plate. Also, $v_0 < 0$ gives blowing whereas $v_0 > 0$ gives suction.

The Eqs. (1)-(5) are reformed into the dimensionless set of ODEs by considering the aforesaid Eqs. (8)-(10) as:

$$(1 + \Delta) f'(\eta) + 2\xi f'(\eta) + Gr\theta(\eta) + Gm\phi(\eta) - Mf(\eta) + \Delta \lambda h'(\eta) = 0 \quad (11)$$

$$\Lambda h'(\eta) - \lambda \lambda_1^2 \left\{ 2h(\eta) + \frac{1}{\lambda_1} f'(\eta) \right\} + 2\xi h'(\eta) = 0 \quad (12)$$

$$\theta'(\eta) + Pr \{ Df\phi'(\eta) + 2\xi \theta'(\eta) \} = 0 \quad (13)$$

$$\phi'(\eta) + 2\xi Sc\phi'(\eta) + Sc Sr\theta'(\eta) = 0 \quad (14)$$

The boundary conditions (6)-(7) are transferred into relations as:

$$\phi(\eta) = 1, f(\eta) = 1, \theta(\eta) = 1, h(\eta) = -sf'(\eta) \text{ at } \eta = 0 \quad (15)$$

$$f(\eta) = 0, \phi(\eta) = 0, \theta(\eta) = 0, h(\eta) = 0 \text{ at } \eta \rightarrow \infty \quad (16)$$

where $Gm = \frac{g\beta^* \nu (C_w - C_\infty)}{U_0^2}$ is the modified local Grashof Number, $Sc = \frac{\nu}{D_m}$ is the Schmidt number, $\Lambda = \frac{\gamma}{\rho j \nu}$ is the spin gradient viscosity, $\lambda_1 = \frac{v_0}{U_0}$ is an arbitrary constant, $Gr = \frac{g\beta \nu (T_w - T_\infty)}{U_0^2}$ is the local Grashof number, $Pr = \frac{\rho \nu C_p}{k}$ is the Prandtl number, $\Delta = \frac{k}{\rho \nu}$ is the micro rotational parameter, $\lambda = \frac{\chi \nu}{\rho j U_0^2}$ is the vortex viscosity, and $\xi = \eta + \frac{v_0}{2}$ is the unsteady parameter.

3. Numerical procedure

The main target is to utilize the Finite difference method (FDM) to find the resolutions of ODEs (11)-(14) including the boundary conditions (15)-(16) in this research. This approach has been demonstrated to be accurate and effective in resolving a variety of problems (Ali et al. [25] and Cheng and Liu [26]). The FMD discretizes the domain space of the solution.

We will apply grid size $\Delta\eta = h > 0$ in η -direction, $\Delta\eta = \frac{1}{N}$, with $\eta_i = ih$ ($i = 0, 1, \dots, N$). Suppose that $f_i = f(\eta_i)$, $\theta_i = \theta(\eta_i)$ and $\phi_i = \phi(\eta_i)$.

Let the functions f , θ , and ϕ have the numerical values as F_i , Θ_i , and Φ_i at the i^{th} node, respectively.

So, we assume:

$$f'_i = \frac{f_{i+1} - f_{i-1}}{2h}, \theta'_i = \frac{\theta_{i+1} - \theta_{i-1}}{2h}, \phi'_i = \frac{\phi_{i+1} - \phi_{i-1}}{2h} \quad (17)$$

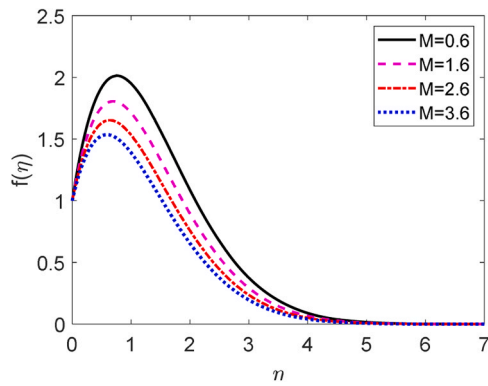


Fig. 2. Velocity profile for M.

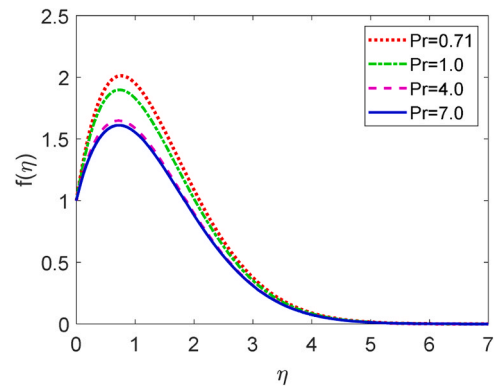


Fig. 4. Velocity profile for Pr.

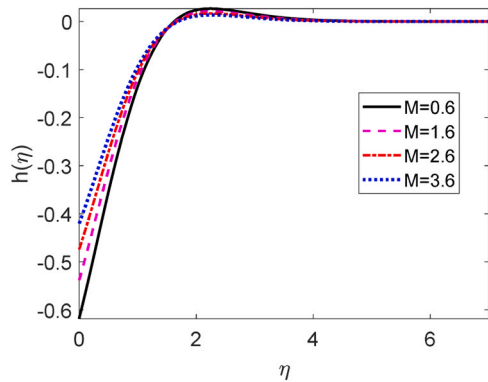


Fig. 3. Microrotation profile for M.

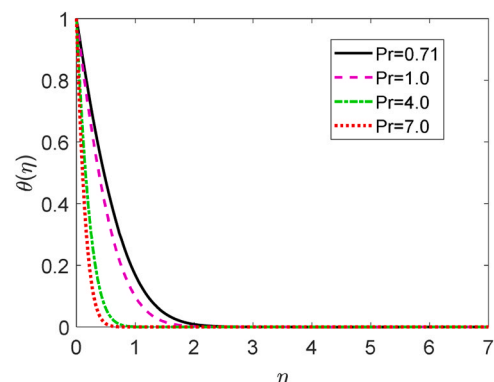


Fig. 5. Temperature profile for Pr.

$$f''|_i = \frac{f_{i+1} - 2f_i + f_{i-1}}{h^2}, \quad \theta''|_i = \frac{\theta_{i+1} - 2\theta_i + \theta_{i-1}}{h^2}, \quad \phi''|_i = \frac{\phi_{i+1} - 2\phi_i + \phi_{i-1}}{h^2} \tag{18}$$

The set of ODES (11)–(14) is discretized within space through the use of FDM and is regarded as the key step. To accomplish this, we have placed (17) - (18) into (11)-(14) and neglected the truncation errors. So, the consequent algebraic equations become:

$$(1 + \Delta)(F_{i+1} - 2F_i + F_{i-1}) + \xi h(F_{i+1} - F_{i-1}) + h^2(Gr\Theta_i + Gm\Phi_i) - Mh^2F_i + \Delta\lambda h(H_{i+1} - H_{i-1}) = 0 \tag{19}$$

$$\Lambda(H_{i+1} - 2H_i + H_{i-1}) - \lambda\lambda_1^2 \left\{ 2h^2H_i + \frac{1}{\lambda_1}h(F_{i+1} - F_{i-1}) \right\} + 2\xi h(H_{i+1} - H_{i-1}) = 0 \tag{20}$$

$$\Theta_{i+1} - 2\Theta_i + \Theta_{i-1} + Pr[\xi h(\Theta_{i+1} - \Theta_{i-1}) + Df(\Phi_{i+1} - 2\Phi_i + \Phi_{i-1})] = 0 \tag{21}$$

$$\Phi_{i+1} - 2\Phi_i + \Phi_{i-1} + Sc[\xi h(\Phi_{i+1} - \Phi_{i-1}) + Sr(\Theta_{i+1} - 2\Theta_i + \Theta_{i-1})] = 0 \tag{22}$$

Also, the boundary conditions are

$$F_0 = 1, \quad \Theta_0 = 1, \quad \Phi_0 = 1, \quad F_N = 0, \quad \Theta_N = 0, \quad \Phi_N = 0 \tag{23}$$

The equations from (19) to (22) including boundary condition (23) represent a nonlinear set of algebraic equations in F_i , Θ_i , and Φ_i . Using MATLAB software and an appropriate starting solution, we will employ the Newton iteration approach in our computation.

Table 1

Impact of the magnetic parameter (M) on $f'(0)$, $h'(0)$, $-\theta'(0)$, and $-\phi'(0)$ when $Pr=0.71$, $Gr=20.0$, $Gm=12.0$, $v_0 = 0.6$, $Sc=0.22$, $Df=0.5$, $Sr=2.0$, $\Delta = 5.0$, $\lambda = 0.5$, and $s=0.2$.

M	$f'(0)$	$h'(0)$	$-\theta'(0)$	$-\phi'(0)$
0.6	3.09254771887805	0.489471867949944	1.23755295167690	0.219818206456390
1.6	2.69190109727656	0.424027493740421	1.23755295167690	0.219818206456390
2.6	2.37070813382750	0.370829839321152	1.23755295167690	0.219818206456390
3.6	2.10246136194693	0.325869983929045	1.23755295167690	0.219818206456390

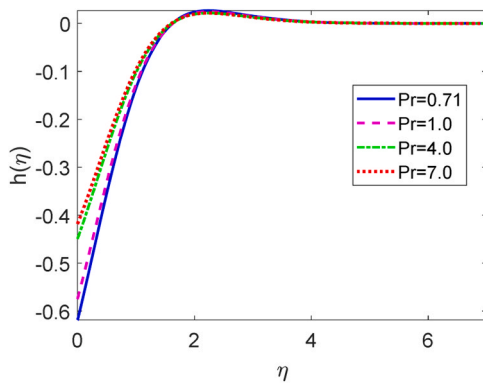


Fig. 6. Microrotation profile for Pr.

4. Results and discussions

An investigation for behavior of micropolar fluid on a unstable MHD forced convection and mass transmission flow passing a permeable medium was carried out to examine the impacts of the micro rotation, vortex viscosity, and spin gradient viscosity considering the influences of magnetic field and suction. For the present analysis, firstly, the nonlinear PDEs (1)-(5) are transformed into simultaneous ODEs (11)-(14) by using similarity variables. The default parameters are taken as: $0.6 \leq M \leq 3.6$, $0.71 \leq Pr \leq 7.0$, $-1.5 \leq v_0 \leq 2.6$, $3.0 \leq \Delta \leq 6.0$, $0.5 \leq Df \leq 4.0$, $0.1 \leq \lambda \leq 1.2$, $1.0 \leq Sr \leq 4.0$, $0.22 \leq Sc \leq 6.7$, $-30.0 \leq Pr \leq 30.0$, and $0.1 \leq s \leq 0.8$.

The important role of magnetic parameter (M) on the angular velocity and velocity fields are manifested in Figs. 2 and 3. This result shows from Fig. 2 that the fluid flow decreases with an increasing in M. When M increases, then the barrier force happens in the computation domain. This barrier force refers to the Lorentz force. The Lorentz force performs like a resistive force which lessens the fluid motion. Thus, Table 1 reveals that the local skin friction reduces for upward quantities of M. From the boundary condition we see that the microrotation starts from negative. This behavior is found in Fig. 3. We also found from Fig. 3 that the microrotation of the fluid improves with the enhance of M within the region $0 \leq \eta \leq 1.2$. Then we also observe from Fig. 3 that the microrotation fields lessen slowly when $\eta > 1.2$ as M is improved.

Figs. 4–6 show the temperature, velocity, and microrotation fields for numerous amounts of the Prandtl number (Pr). The kinematic viscosity is proportionate to Pr. When the values of Pr enhances, the kinematic viscosity augments within the computational domain. So, the fluid motion is observed to decrease monotonically as shown in Fig. 4. For this reason, the thin boundary layer representing the decay of natural convection. With the improvement of Pr, the thermal boundary layer becomes thinner owing to the reduction in the temperature field as illustrated in Fig. 5. The heat transmission rate goes up for growing amounts of Pr as shown in Table 2. Physically, large heat capacity comes from a fluid with a large Prandtl number and hence improves the heat transmission rate. Fig. 6 demonstrates that the microrotation profile enhances within the region $0 \leq \eta \leq 1.9$ with the improving amounts of Pr. Then, we also observe as in Fig. 6 that the microrotation of the fluid uniforms for $\eta > 2.2$ an improvement of Pr.

Table 2

Effect of the Prandtl number (Pr) on $f'(0)$, $h'(0)$, $-\theta'(0)$, and $-\phi'(0)$ when $Pr=0.71$, $Gr=20.0$, $Gm=12.0$, $v_0 = 0.6$, $Sc=0.22$, $Df=0.5$, $Sr=2.0$, $\Delta = 5.0$, $\lambda = 0.5$, and $s=0.2$.

Pr	$f'(0)$	$h'(0)$	$-\theta'(0)$	$-\phi'(0)$
0.71	3.09254771887805	0.489471867949944	1.23755295167690	0.219818206456390
1.0	2.87359503554895	0.450653350493341	1.53604708357502	0.219818206456390
4.0	2.24692377698426	0.332918894534006	3.97453255494882	0.219818206456390
7.0	2.08993740844637	0.301657053354658	6.07681487903149	0.219818206456390

Figs. 7–10 indicate the microrotation, concentration temperature and velocity fields for several amounts of suction parameter (v_0). When $v_0 > 0$ then the suction happens in the computational domain but $v_0 < 0$ shows the blowing (injection) at the sheet. The fluid motion diminishes

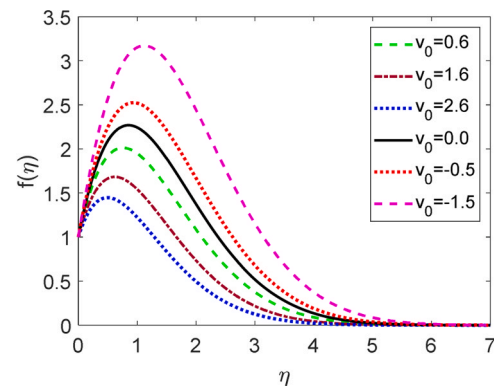


Fig. 7. Velocity profile for v_0 .

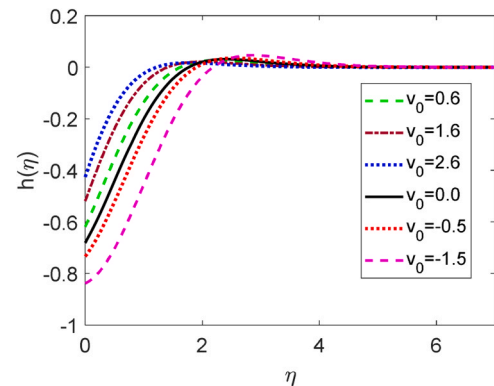


Fig. 8. Microrotation profile for v_0 .

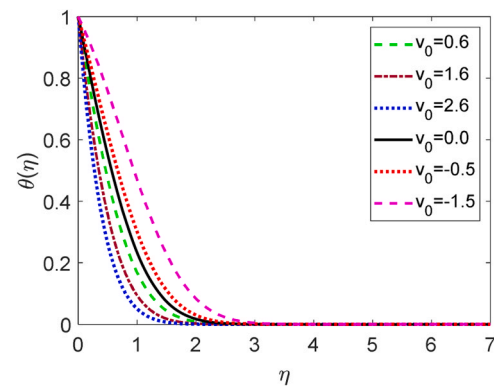


Fig. 9. Temperature profile for v_0 .

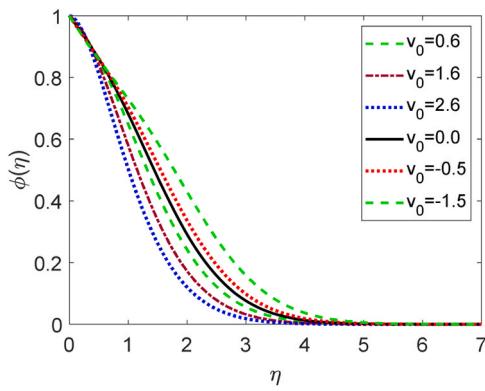


Fig. 10. Concentration profile for v_0 .

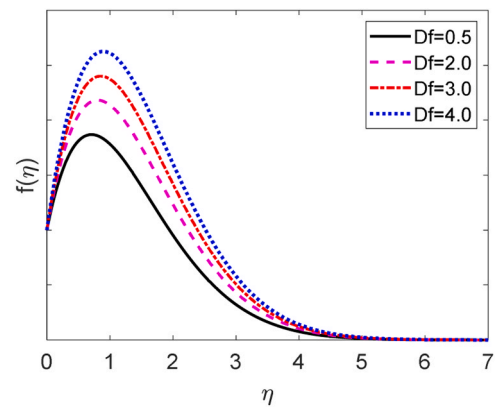


Fig. 13. Velocity profile for Df .

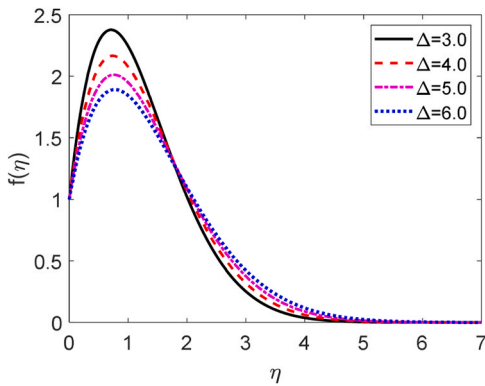


Fig. 11. Velocity profile for Δ .

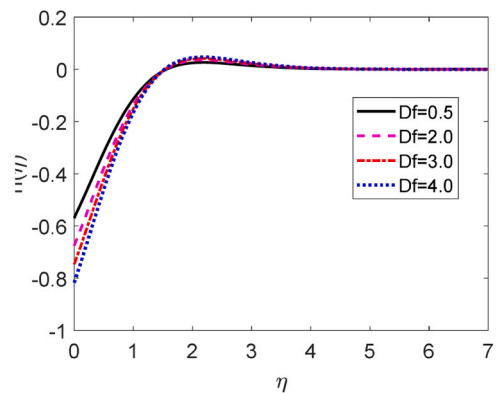


Fig. 14. Microrotation profile for Df .

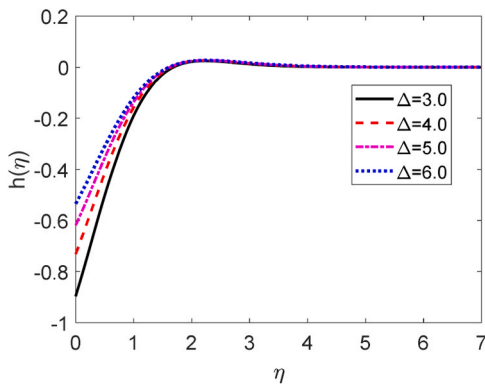


Fig. 12. Microrotation profile for Δ .

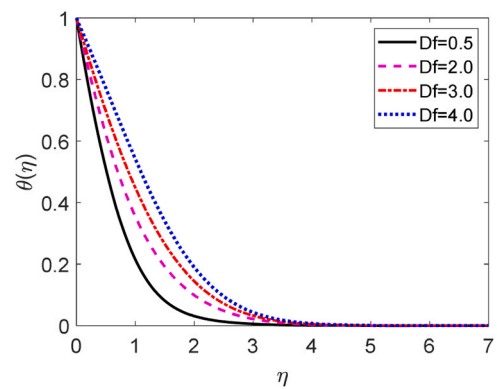


Fig. 15. Temperature profile for Df .

for uprisng amounts of v_0 . Suction means some fluids extracted from the computational domain. Blowing is the process of injecting fluids into the computational domain. Consequently, the fluid speed develops for improving quantities of the blowing parameter. This is because that the suction or blowing signifying the fact that v_0 steadies the growth of the boundary layer. As η rises from 0 to ∞ , Fig. 8 specifies that the angular velocity, or microrotation field, turns into negative and advances from the wall to zero. Fig. 8 states that the microrotation of the fluid has tendency to become positive for improving values of v_0 . The heat transmission rate develops for growing quantities of v_0 . For this reason, the fluid temperature decays for v_0 as shown in Fig. 9. The same behavior is observed for concentration as located in Fig. 10.

The important influence of the microrotation parameter (Δ) on the microrotation and velocity fields are demonstrated in Figs. 11 and 12. Figure shows that the fluid velocity enhances firstly in the region $0 <$

$\eta < 0.9$ as Δ improves. Later, fluid speed gradually lessens for $\eta > 1$ as Δ is advanced. Fig. 12 illustrates that for rising amounts of Δ , the angular velocity begins negatively and improves inside the boundary layer.

Figs. 13–15 interpret the microrotation, velocity, and temperature fields for numerous quantities of Dufour number (Df). The relationship between the Dufour number and the kinematic viscosity is well defined as being directly inversely proportional. When Dufour number improves in the computational region, the kinematic viscosity falls down. So, the frictional force decays for growing values of Df . For this reason, the fluid motion lessens for Df as shown in Fig. 13. The angular velocity starts negative and reduces within the region $0 < \eta < 1.8$ with an increase in Df as plotted in Fig. 14. Additionally, Fig. 14 states that the microrotation distribution improves slowly for $\eta > 1.8$ as the increase of Df . We are aware that the thermal diffusion (k_r) and the Dufour number

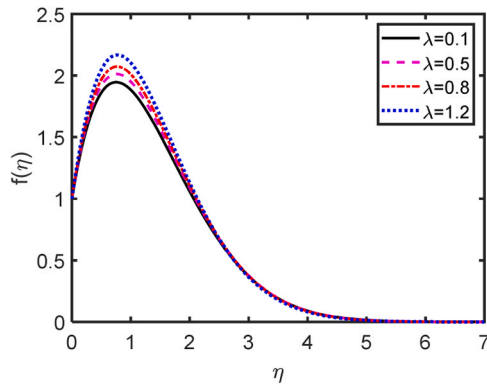


Fig. 16. Velocity profile for λ .

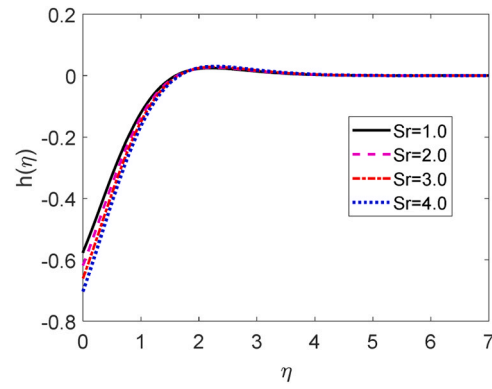


Fig. 19. Microrotation profile for Sr.

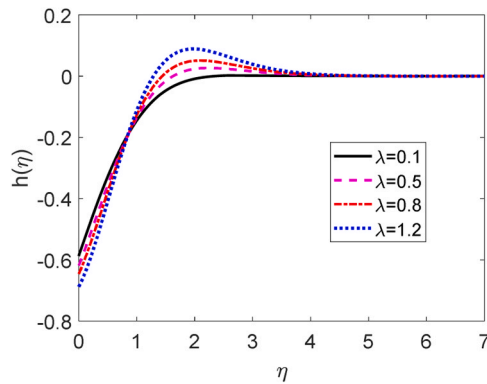


Fig. 17. Microrotation profile for λ .

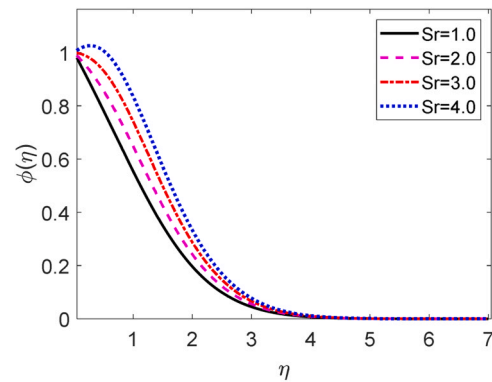


Fig. 20. Concentration profile for Sr.

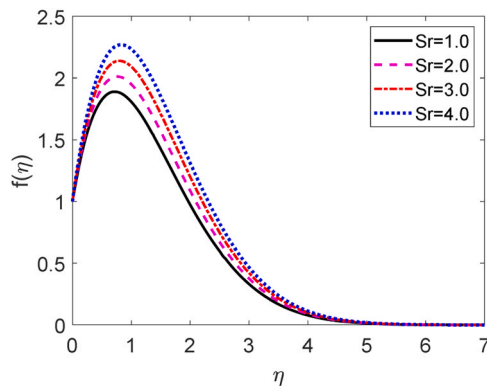


Fig. 18. Velocity profile for Sr.

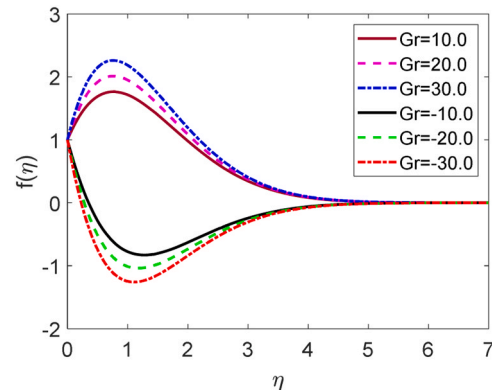


Fig. 21. Velocity profile for Gr.

(Df) are proportional to each other. The heat transmission rate diminishes for growing quantities of Df. The thermal boundary layer thickness enhances for Df. For this reason, the fluid temperature improves for moving amounts of Df as explored in Fig. 15.

The important role of the vortex viscosity parameter (λ) on the microrotation and velocity distributions are shown in Figs. 16 and 17. It is discovered that near the leading edge within the zone $0 < \eta < 0.8$, the velocity profile first gets slightly better as the improving amounts of λ as shown in Fig. 16 and later, velocity distribution gradually diminishes for $\eta > 1$. With the exception of the area immediately near the wall, where kinematic viscosity predominates in the flow, the angular velocity advances with rising amounts of λ components, as demonstrated in Fig. 17.

The impact of the Soret number (Sr) on the concentration, velocity, and microrotation fields are displayed in Figs. 18–20. Fig. 18 reveals

that the velocity distribution enhances with the improving amounts of Sr. The kinematic viscosity and the Soret number are known to be inversely related. The viscose force less dominant in the computational domain for growing values of Sr. The microrotation distribution starts negative and decays in the region $0 < \eta < 2$ for mounting amounts of Sr as shown in Fig. 19. After this region the microrotation field uniforms for Sr as $\eta \rightarrow \infty$. We also see from this Fig. 20 that the concentration field rises with the upsurge of Sr. Because the Soret number varies as per the mass diffusivity. It means that the mass transmission rate diminishes for upward amounts of Sr as shown in Table 7.

Figs. 21 and 22, respectively, display the effect various quantities of the local Grashof number (Gr) on the velocity and microrotational fields. When Gr is small ($Gr \ll 1$), it indicates that viscous forces are predominant, and the fluid flow will be relatively slow and stable. In such

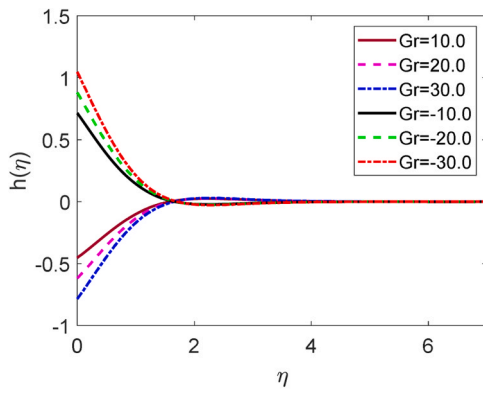


Fig. 22. Microrotation profile for Gr.

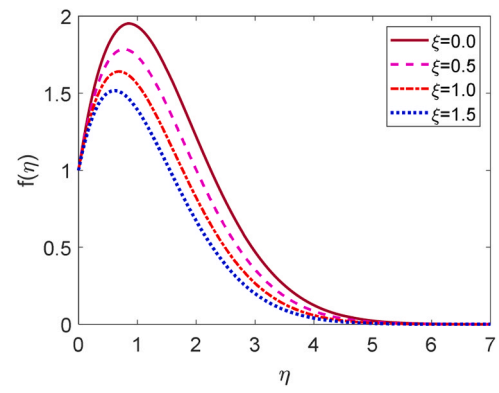


Fig. 25. Velocity profile for ξ .

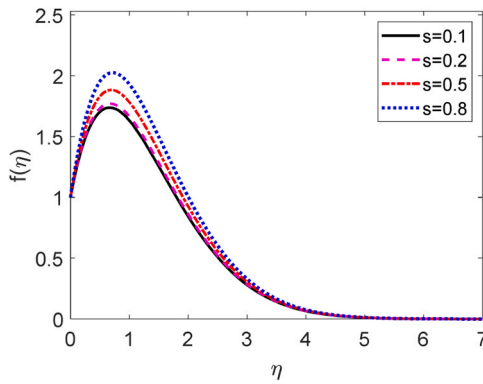


Fig. 23. Velocity profile for s.

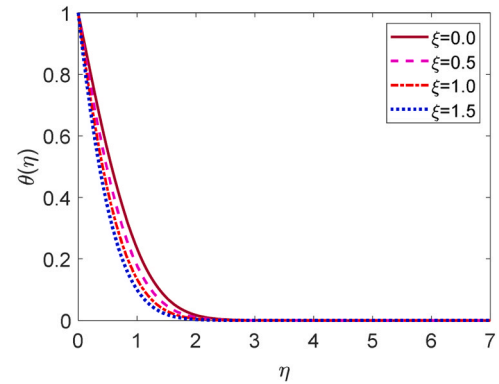


Fig. 26. Temperature profile for ξ .

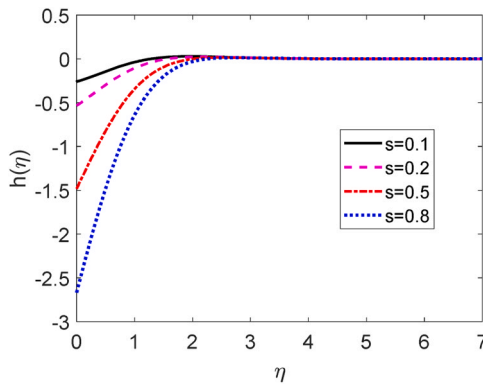


Fig. 24. Microrotation profile for s.

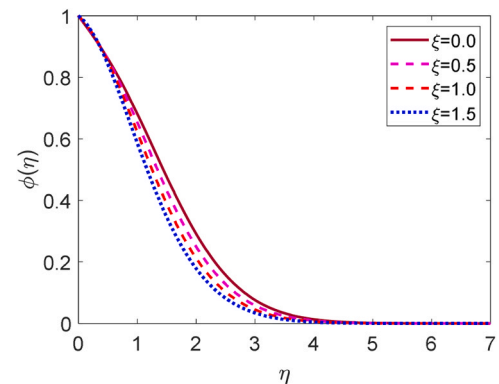


Fig. 27. Concentration profile for ξ .

cases, the temperature differences within the fluid are not sufficient to overcome the inhibiting effects of viscosity, resulting in limited convective motion. On the other hand, when Gr is large ($Gr \gg 1$), buoyancy forces become dominant. In this regime, temperature differences drive strong convective currents within the fluid, leading to more rapid and vigorous fluid motion. This can result in the formation of convection cells or plumes, which are characteristic patterns of fluid flow in natural convection as shown in Fig. 21. But the opposite behavior is found for the microrotation field as revealed in Fig. 22.

The consequences of the constant (s) on the microrotation and velocity outlines are plotted in Figs. 23 and 24. The Figures demonstrate that the fluid motion develops but the microrotation reduces for growing values of s. When $s=0$ the boundary condition indicates the no-spin condition.

Figs. 25–28 shows the effect of the unsteady parameter (ξ) on the velocity, temperature, concentration as well as Microrotation,

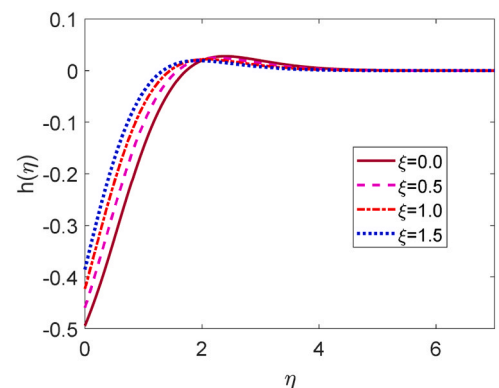


Fig. 28. Microrotation profile for ξ .

Table 3

Effect of the suction parameter (v_0) on $f'(0)$, $h'(0)$, $-\theta'(0)$, and $-\phi'(0)$ when $Pr=0.71$, $Gr=20.0$, $Gm=12.0$, $v_0 = 0.6$, $Sc=0.22$, $Df=0.5$, $Sr=2.0$, $\Delta = 5.0$, $\lambda = 0.5$, and $s=0.2$.

v_0	$f'(0)$	$h'(0)$	$-\theta'(0)$	$-\phi'(0)$
3.0	1.95335782849629	0.707725806797194	2.60535751775987	0.00876205626483895
2.0	2.40349630799681	0.655371114968655	2.00275565186992	0.0946660248892579
0.6	3.09254771887805	0.489471867949944	1.23755295167690	0.219818206456390
0.0	3.40558196543032	0.389969785215887	0.950789185735497	0.260511275481077
-0.5	3.67060980690463	0.297683349763562	0.736914558193017	0.285545217770891
-1.0	3.93482581846832	0.200249318551391	0.549562886504191	0.300743721001730

Table 4

Effect of the Schmidt number (Sc) on $f'(0)$, $h'(0)$, $-\theta'(0)$, and $-\phi'(0)$ when $Pr=0.71$, $Gr=20.0$, $Gm=12.0$, $v_0 = 0.6$, $Sc=0.22$, $Df=0.5$, $Sr=2.0$, $\Delta = 5.0$, $\lambda = 0.5$, and $s=0.2$.

Sc	$f'(0)$	$h'(0)$	$-\theta'(0)$	$-\phi'(0)$
0.22	3.09254771887805	0.489471867949944	1.23755295167690	0.219818206456390
0.33	2.92124227381472	0.473773570727862	1.23755295167690	0.214181302112946
0.50	2.77808189608025	0.460128306710922	1.23755295167690	0.188809978259071
0.67	2.69581788004750	0.452070482542075	1.23755295167690	0.153963408838732

Table 5

Effect of the micro rotational parameter (Δ) on $f'(0)$, $h'(0)$, $-\theta'(0)$, and $-\phi'(0)$ when $Pr=0.71$, $Gr=20.0$, $Gm=12.0$, $v_0 = 0.6$, $Sc=0.22$, $Df=0.5$, $Sr=2.0$, $\Delta = 5.0$, $\lambda = 0.5$, and $s=0.2$.

Δ	$f'(0)$	$h'(0)$	$-\theta'(0)$	$-\phi'(0)$
3.0	4.48030696168514	0.751228003326456	1.23755295167690	0.219818206456390
4.0	3.65511997565085	0.595270386606995	1.23755295167690	0.219818206456390
5.0	3.09254771887805	0.489471867949944	1.23755295167690	0.219818206456390
6.0	2.67209298640757	0.410728867608023	1.23755295167690	0.219818206456390

Table 6

Effect of the vortex viscosity (λ) on $f'(0)$, $h'(0)$, $-\theta'(0)$, and $-\phi'(0)$ when $M=0.6$, $Gr=20.0$, $Gm=12.0$, $Pr = 0.71$, $v_0=0.6$, $Df=0.5$, $Sr=2.0$, $Sc = 0.22$, $\Delta = 5.0$, and $s=0.2$.

λ	$f'(0)$	$h'(0)$	$-\theta'(0)$	$-\phi'(0)$
0.1	2.93267388435562	0.560629801538832	1.23755295167690	0.219818206456390
0.5	3.09254771887805	0.489471867949944	1.23755295167690	0.219818206456390
0.8	3.22838610844691	0.434797884884948	1.23755295167690	0.219818206456390
1.2	3.43585039957000	0.360050114323186	1.23755295167690	0.219818206456390

Table 7

Effect of the Soret number (Sr) on $f'(0)$, $h'(0)$, $-\theta'(0)$, and $-\phi'(0)$ when $Pr=0.71$, $Gr=20.0$, $Gm=12.0$, $v_0 = 0.6$, $Sc=0.22$, $Df=0.5$, $Sr=2.0$, $\Delta = 5.0$, $\lambda = 0.5$, and $s=0.2$.

Sr	$f'(0)$	$h'(0)$	$-\theta'(0)$	$-\phi'(0)$
1.0	2.88132439443914	0.466927184161096	1.23755295167690	0.417936560132386
2.0	3.09254771887805	0.489471867949944	1.23755295167690	0.219818206456390
3.0	3.30377104004743	0.512016548923374	1.23755295167690	0.0216998519952838

respectively. It is clearly observed from these figures that the fluid velocity, temperature and concentration for higher values of the unsteady parameter. But the opposite behavior is found for microrotation.

Tables 1–7, respectively, reveal the properties of the various dimensionless parameters/ numbers on the surface couple stress ($h'(0)$), local skin friction ($f'(0)$), heat transmission rate ($-\theta'(0)$), and mass transmission rate ($-\phi'(0)$). It is found from these above Tables that ($f'(0)$) advances for upward amounts of vortex viscosity (λ) and Soret number (Sr). But the opposite behavior is happened for moving values of Prandtl number (Pr), Schmidt number (Sc), magnetic parameter (M), suction parameter (v_0), and the micro rotational parameter (Δ). The values of ($f'(0)$) improve by around 17%, and 15% for growing levels of λ (0.1–1.2), and Sr (1.0–3.0), respectively. On the other hand, the values of ($f'(0)$) decay by around 32%, 32%, 37%, 13%, and 40% due to increasing values of M from 0.6 to 3.6, Pr from 0.71 to 7.0, v_0 from 0.6 to 3.0, Sc from 0.22 to 0.67, and Δ from 3.0 to 6.0, respectively. The heat

transmission rate enhances for growing levels of Pr from 0.71 to 7.0 and v_0 from 0.6 to 3.0. The heat transmission rate develops by around 391%, and 110% for rising amounts of Pr from 0.71 to 7.0, and v_0 from 0.6 to 3.0, respectively. The values of ($h'(0)$) decline for uprising quantities of M , Pr , Δ , λ , and Sc . But the reverse impact is detected for v_0 and Sr . The values of ($h'(0)$) decay by around 33%, 38%, 8%, 45%, and 36% due to increasing values of M from 0.6 to 3.6, Pr from 0.71 to 7.0, Sc from 0.22 to 0.67, Δ from 3.0 to 6.0, and λ from 0.1 to 1.2, respectively. But, rising values of v_0 from 0.6 to 3.0, and Sr from 1.0 to 3.0 improve the values of ($h'(0)$) by around 45%, and 10%, respectively.

5. Comparison

The outcomes of this present paper are compared with Hasanuzzaman et al. [10]. The comparison of $f'(0)$, and $-\theta'(0)$ are plotted in Table 8. Our numerical findings and Hasanuzzaman et al. [10] are found

Table 8

Comparison of $-\theta'(0)$, and $-\phi'(0)$ when $N = 0.0$.

M	Sc	$-\theta'(0)$ Hasanuzzaman et al. [10]	$-\theta'(0)$ Present Study	$-\phi'(0)$ Hasanuzzaman et al. [10]	$-\phi'(0)$ Present Study
0.5	1.0	1.419837	1.419216	0.221873	0.227531
1.0	1.0	1.419841	1.418937	0.221885	0.227685
0.5	2.0	1.3539478	1.352157	0.780809	0.779591

to have the best agreement.

6. Conclusions

The influences of the suction and the Lorentz force upon unstable MHD-free convective and mass transmission flow of micropolar liquid passing a permeable plate were discussed in this article. It is possible to reach the following conclusions:

- The fluid motion lessens for rising levels of the micro rotational parameter.
- The microrotation decays with an increase of the dominant parameters.
- The heat transmission rate advances for growing levels of Pr resulting a reduction in temperature ($0.71 \leq Pr \leq 1.0$).
- As the Schmidt number goes up, the molecular diffusivity of the chemical species drops ($0.22 \leq Sc \leq 0.67$).

The findings of this study could be beneficial for boundary layer domination in the field of aerodynamics as well plasma studies, liquid crystals, lubrication geo-thermal energy extractions, blood, in power engineering, and generators etc.

Declaration of Competing Interest

The authors declare that they have no known competing financial interests or personal relationships that could have appeared to influence the work reported in this paper.

References

- [1] A.C. Eringen, Theory of micropolar fluids, *J. Math. Mech.* (1966) 1–18.
- [2] B.C. Sakiadis, Boundary layer behavior on a continuous solid surface; the boundary layer on a continuous moving surface, *AIChE J.* 7 (1961) 26–28.
- [3] G. Ahmadi, Self-similar solution of incompressible micropolar boundary layer flow over a semi-infinite plate, *Int. J. Eng. Sci.* 14 (7) (1976) 639–646.
- [4] S.K. Jena, M.N. Mathur, Similarity solutions for laminar free convection flow of a thermomicrofluid past a non-isothermal vertical flat plate, *Int. J. Eng. Sci.* 19 (11) (1981) 1431–1439.
- [5] O. Ojjela, N. Naresh Kumar, Unsteady MHD flow and heat transfer of micropolar fluid in a porous medium between parallel plates, *Can. J. Phys.* 93 (8) (2015) 880–887.
- [6] M. Ashraf, A.R. Wehgal, MHD flow and heat transfer of micropolar fluid between two porous disks, *Appl. Math. Mech.* 33 (2012) 51–64.
- [7] S. Nadeem, M. Hussain, M. Naz, MHD stagnation flow of a micropolar fluid through a porous medium, *Meccanica* 45 (2010) 869–880.
- [8] Rahman, M.M., & Sattar, M.A. (2006). Magnetohydrodynamic convective flow of a micropolar fluid past a continuously moving vertical porous plate in the presence of heat generation/absorption.
- [9] P.O. Olanrewaju, G.T. Okedayo, J.A. Gbadeyan, Effects of thermal radiation on magnetohydrodynamic flow of a micropolar fluid towards a stagnation point on a vertical plate, *Int. J. Appl. Sci. Technol.* 1 (6) (2011) 1–6.
- [10] M. Hasanuzzaman, M.A.K. Azad, M.M. Hossain, Effects of Dufour and thermal diffusion on unsteady MHD free convection and mass transfer flow through an infinite vertical permeable sheet, *SN Appl. Sci.* 3 (12) (2021) 882.
- [11] M. Hasanuzzaman, S. Sharin, T. Hassan, M.A. Kabir, R. Afroj, A. Miyara, Unsteady magneto-convective heat-mass transport passing in a vertical permeable sheet with internal heat generation effect, *Transp. Eng.* 9 (2022) 100126.
- [12] M. Hasanuzzaman, S. Akter, S. Sharin, M.M. Hossain, A. Miyara, M.A. Hossain, Viscous dissipation effect on unsteady magneto-convective heat-mass transport passing in a vertical porous plate with thermal radiation, *Heliyon* 9 (2023) 3.
- [13] M.G. Reddy, N.B. Reddy, Soret and Dufour effects on steady MHD free convection flow past a semi-infinite moving vertical plate in a porous medium with viscous dissipation, *Int. J. Appl. Math. Mech.* 6 (1) (2010) 1–12.
- [14] O. Ojjela, N. Naresh Kumar, Unsteady MHD mixed convection flow of chemically reacting micropolar fluid between porous parallel plates with soret and dufour effects, *J. Eng.* (2016) 2016.
- [15] S.R. Sheri, M.D. Shamsuddin, Heat and mass transfer on the MHD flow of micro polar fluid in the presence of viscous dissipation and chemical reaction, *Procedia Eng.* 127 (2015) 885–892.
- [16] H. Mirgolbabaee, S.T. Ledari, D.D. Ganji, Semi-analytical investigation on micropolar fluid flow and heat transfer in a permeable channel using AGM, *J. Assoc. Arab Univ. Basic Appl. Sci.* 24 (2017) 213–222.
- [17] S. Ahmad, M. Ashraf, K. Ali, Numerical simulation of viscous dissipation in a micropolar fluid flow through a porous medium, *J. Appl. Mech. Tech. Phys.* 60 (2019) 996–1004.
- [18] M.E. Ghoneim, Z. Khan, S. Zuhra, A. Ali, E. Tag-Eldin, Numerical solution of Rosseland's radiative and magnetic field effects for Cu-Kerosene and Cu-water nanofluids of Darcy-Forchheimer flow through squeezing motion, *Alex. Eng. J.* 64 (2023) 191–204.
- [19] Z. Khan, S. Zuhra, S. Islam, M.A.Z. Raja, A. Ali, Modeling and simulation of Maxwell nanofluid flows in the presence of Lorentz and Darcy-Forchheimer forces: toward a new approach on Buongiorno's model using artificial neural network (ANN), *Eur. Phys. J.* 138 (1) (2023) 107.
- [20] Z.S. Hosseini, A. Abidi, S. Mohammadi, S.A.M. Mehryan, C. Hulme, A fully resolved computational fluid dynamics study of the boundary layer flow of an aqueous nanoliquid comprising gyrotactic microorganisms over a stretching sheet: the validity of conventional similarity models, *Mathematics* 9 (21) (2021) 2655.
- [21] M. Izadi, M.A. Sheremet, S.A.M. Mehryan, I. Pop, H.F. Öztop, N. Abu-Hamdeh, MHD thermogravitational convection and thermal radiation of a micropolar nanoliquid in a porous chamber, *Int. Commun. Heat. Mass Transf.* 110 (2020) 104409.
- [22] M.V. Krishna, P.V.S. Anand, A.J. Chamkha, Heat and mass transfer on free convective flow of a micropolar fluid through a porous surface with inclined magnetic field and hall effects, *Spec. Top. Rev. Porous Media.: Int. J.* 10 (3) (2019).
- [23] M.V. Krishna, K. Bharathi, A.J. Chamkha, Hall effects on MHD peristaltic flow of Jeffrey fluid through porous medium in a vertical stratum, *Interfacial Phenom. Heat. Transf.* 6 (3) (2018).
- [24] P.K. Pattnaik, D.K. Moapatra, S.R. Mishra, Influence of velocity slip on the MHD flow of a micropolar fluid over a stretching surface. In *Recent Trends in Applied Mathematics: Select Proceedings of AMSE 2019*, Springer Singapore, 2021, pp. 307–321.
- [25] P. Mathur, S.R. Mishra, P.K. Pattnaik, R.K. Dash, Characteristics of Darcy-Forchheimer drag coefficients and velocity slip on the flow of micropolar nanofluid, *Heat. Transf.* 50 (7) (2021) 6529–6547.
- [26] M.Z. Haque, M.M. Alam, M. Ferdows, A. Postelnicu, Micropolar fluid behaviors on steady MHD free convection and mass transfer flow with constant heat and mass fluxes, joule heating and viscous dissipation, *J. King Saud. Univ. -Eng. Sci.* 24 (2012) 71–84.
- [27] J.C. Ali, E.A. Sameh, S.A. Abdulkareem, Melting and radiation effects on mixed convection from a vertical surface embedded in a non-Newtonian fluid saturated non-Darcy porous medium for aiding and opposing external flows, *Int. J. Phys. Sci.* 5 (7) (2010) 1212–1224.
- [28] W.T. Cheng, C.H. Lin, Unsteady mass transfer in mixed convective heat flow from a vertical plate embedded in a liquid-saturated porous medium with melting effect, *Int. Commun. Heat. Mass Transf.* 35 (10) (2008) 1350–1354.